References
Day, J. (1979) Ph.D. Thesis, Boston University, Boston, MA.
Gaber, B. P., & Peticolas, W. L. (1977) *Biochim. Biophys. Acta 465*, 260.
Gaber, B. P., Yager, P., & Peticolas, W. L. (1978a) *Biophys. J. 21*, 161.
Gaber, B. P., Yager, P., & Peticolas, W. L. (1978b) *Biophys. J. 22*, 191.
Gaber, B. P., Yager, P., & Peticolas, W. L. (1978c) *Biophys. J. 24*, 677.
Gordon, R. G. (1965) *J. Chem. Phys. 43*, 1307.
Gotoh, R., & Takaneka, T. (1961) *Bull. Inst. Chem. Res., Kyoto Univ. 39*, 202.
Hubbell, W. L., & McConnell, H. M. (1971) *J. Am. Chem. Soc. 93*, 314.
Levine, Y. K., Birdsall, N. J. M., Lee, A. G., & Metcalfe, J. C. (1972) *Biochemistry 11*, 1416.
Mendelsohn, R., & Maisano, J. (1978) *Biochim. Biphys. Acta 506*, 192.
Mendelsohn, R., Sunder, S., & Bernstein, H. J. (1976) *Biochim. Biophys. Acta 443*, 613.
Metcalfe, J. C., Birdsall, N. J. M., Feeney, J., Lee, A. G., Levine, Y. K., & Partington, P. (1971) *Nature (London) 233*, 199.
Mizushima, S. I., & Shimanouchi, T. (1949) *J. Am. Chem. Soc. 71*, 1320.
Oldfield, E., Gutowsky, H. S., Hshung, J. C., Jacobs, R. E., Kang, S. Y., King, T. E., Meadows, M. D., & Rice, D. M. (1978a) *Proc. Natl. Acad. Sci. U.S.A. 75*, 4657.
Oldfield, E., Meadows, M., Rice, D., & Jacobs, R. (1978b) *Biochemistry 17*, 2727.
Seelig, J. (1977) *Q. Rev. Biophys. 10*, 353.
Smith, I. C. P. (1972) in *Biological Applications of Electron Spin Resonance* (Swartz, H. M., Bolton, J. R., & Borg, D. C., Eds.) pp 483–539, Wiley-Interscience, New York.
Snyder, R. G., Hsu, S. L., & Krimm, S. (1978) *Spectrochim. Acta, Part A 34*, 395.
Spiker, R. C., & Levin, I. W. (1976) *Biochim. Biophys. Acta 433*, 457.
Sunder, S., Mendelsohn, R., & Bernstein, H. J. (1976) *Chem. Phys. Lipids 17*, 456.
Sykora, S. (1972) *J. Chem. Phys. 57*, 1795.
Verma, S. P., & Wallach, D. F. H. (1975) *Biochim. Biophys. Acta 401*, 168.
Wilson, E. B., Jr., Decius, J. C., & Cross, P. C. (1955) *Molecular Vibrations*, pp 69–76, McGraw-Hill, New York.
Yellin, N., & Levin, I. W. (1977) *Biochemistry 16*, 642.

Cholesterol–Phosphatidylcholine Interactions in Multilamellar Vesicles†

Barry R. Lentz,* David A. Barrow, and Mathias Hoechli

ABSTRACT: We have investigated the phase behavior of dipalmitoylphosphatidylcholine–cholesterol bilayers using both the fluorescence of bilayer-associated 1,6-diphenyl-1,3,5-hexatriene (DPH) and freeze–fracture electron microscopy to elucidate specimen structure. Arrhenius analysis of the fluorescence-derived "microviscosity" parameter reveals temperature-induced structural changes in these membranes. In addition, isotherms of DPH fluorescence anisotropy and total intensity are used to detect alterations in membrane structure with varying cholesterol content. Freeze–fracture electron microscopic studies, utilizing rapid "jet-freezing" techniques, show strikingly different fracture-face morphologies for different combinations of sample cholesterol content and temperature. A phase diagram is proposed that offers a unifying interpretation of the fluorescence and freeze–fracture results. In this interpretation, inflections in temperature-scanning and isothermal fluorescence measurements reveal phase lines in the dipalmitoylphosphatidylcholine–cholesterol membranes. Two-phase regions of the proposed phase diagram correspond to samples showing two coexisting fracture-face morphologies, while single-phase regions produce membranes having only one clearly identifiable structure. The proposed phase diagram provides an explanation for several conflicting literature proposals of stoichiometries for phosphatidylcholine–cholesterol complexes in membranes. These stoichiometric complexes correspond to the boundaries of two-phase areas in the gel region of the phase diagram. To better approximate the effect of cholesterol on natural membranes, the structure of egg phosphatidylcholine–cholesterol multilamellar vesicles was also investigated by using DPH fluorescence. The results for this complex natural phospholipid system are interpreted by comparison with the synthetic phospholipid results.

Cholesterol is a major lipid component of many mammalian cell membranes. In humans, it has long been implicated in the etiology of atherosclerosis. For these reasons, research aimed at defining the interaction of cholesterol with phospholipids has been active for two decades [for a recent review, see Demel & DeKruijff (1976)]. Two lipid systems have most often been studied: egg phosphatidylcholine–cholesterol and dipalmitoylphosphatidylcholine (DPPC)[1]–cholesterol mixtures. Usually, these lipid mixtures have been incorporated into either small, unilamellar vesicles or large, multilamellar vesicles. A variety of physical methods have been used to monitor

† From the Department of Biochemistry and Nutrition (B.R.L. and D.A.B.) and the Department of Anatomy (M.H.), University of North Carolina at Chapel Hill, Chapel Hill, North Carolina 27514. *Received September 19, 1979.* Supported by grants from the North Carolina Heart Association, the American Cancer Society (IN-15-R), and the National Science Foundation (PCM76-16761 to B.R.L. and PCM77-20689 to C. R. Hackenbrock). A preliminary account of this work was presented at the 1979 meeting of the Biophysical Society in Atlanta, GA.

[1] Abbreviations used: DPH, 1,6-diphenyl-1,3,5-hexatriene; DPPC, 1,2-dipalmitoyl-3-*sn*-phosphatidylcholine; Tempo, 2,2,6,6-tetramethylpiperidinyl-1-oxy.

0006-2960/80/0419-1943$01.00/0

structure within the different model membrane systems.

Despite these considerable efforts, there is as yet no unifying picture to explain the effects of cholesterol on the phosphatidylcholine bilayer structure. Several reports have proposed that specific complexes or domains are induced in membranes by the presence of cholesterol (Ladbrooke et al., 1968; Engelman & Rothman, 1972; Shimshick & McConnell, 1973; Phillips & Finer, 1974; Estep et al., 1978; Martin & Yeagle, 1978). Unfortunately, a variety of stoichiometries have been suggested for these complexes (e.g., 7.5, 20, 22, 25, 30, 33, 47, and 50 mol % cholesterol). Others have argued against specific complex formation (Stockton & Smith, 1976; Jacobs & Oldfield, 1979) or have presented alternative interpretations of observed structural changes (Huang et al., 1974; Newman & Huang, 1975). These disparate points of view may result from the fact that several distinct phosphatidylcholine–cholesterol model membranes have been studied at different temperatures and compositions by a variety of techniques.

We believe that the complexity of the cholesterol–phosphatidylcholine interaction demands an extensive investigation of one model membrane system by several techniques if a unifying interpretation is to be found. The present report is limited primarily to DPPC–cholesterol large, multilamellar vesicles. DPPC has been chosen as a well-defined, single-component phospholipid species widely used in model membrane studies. In addition, the more complex egg phosphatidylcholine–cholesterol system is also briefly considered and compared to the DPPC–cholesterol system.

We assume that membrane domains should be distinguishable as thermodynamically distinct phases. Our procedure, then, was to study cholesterol–phosphatidylcholine model membranes over an extensive temperature–composition grid and thereby to construct a temperature–composition phase diagram. To detect phase changes, we chose the hydrophobic probe 1,6-diphenyl-1,3,5-hexatriene (DPH).[1] Measurement of the fluorescence anisotropy of membrane-associated DPH provides a rapid, sensitive, and easily interpretable measure of membrane structure (Lentz et al., 1976), thus making possible the investigation of an extensive temperature–composition grid. Simultaneous measurement of light scattering induced depolarization of DPH fluorescence yields an additional parameter sensitive to specimen structure. In order to visualize the phase behavior of DPPC–cholesterol multilamellar vesicles, we used freeze–fracture electron microscopy to determine conditions resulting in the coexistence of different membrane structures. The phase diagram derived from these data offers a unifying model for the interaction of cholesterol with a saturated phosphatidylcholine. It provides a framework within which to design further studies of this and unsaturated model systems by other experimental techniques. Only through such a systematic approach will we learn how cholesterol affects the lipid bilayers of mammalian membranes.

Materials and Methods

Lipids. DPPC was synthesized by the method of Robles & Van den Berg (1969) from palmitic acid (99+%, Sigma Chemical Co.) and glycerol phosphorylcholine (Chadha, 1970) and purified to better than 99%, as established by thin-layer chromatographic analysis (Lentz et al., 1976).

Phosphatidylcholine was isolated from fresh egg yolks (Singleton et al., 1965; Newman & Huang, 1975). The purified material gave only one spot in thin-layer chromatography with Quantum Q5 plates loaded with 1–2 μmol of phospholipid and developed in chloroform–methanol–water (65:25:4). The fatty acid composition was determined by transesterification with methanolic HCl (Stoffel et al., 1959) and separation of the methyl esters on a 10% Silar 10C (Applied Science) column operating in a Perkin-Elmer 900 gas chromatograph. Major fatty acid constituents were $C_{16:0}$ (27 wt %), $C_{18:0}$ (11 wt %), $C_{18:1}$ (39 wt %), $C_{18:2}$ (14 wt %), and others (9%). The purified phosphatidylcholine was found to demonstrate an oxidation index of 0.15 (Klein, 1970), indicating very low levels of acyl-chain oxidation.

Cholesterol was purchased from Fisher Scientific and purified via the dibromide form (Schwenk & Werthessen, 1952). [4-^{14}C]Cholesterol was purchased from New England Nuclear (Lot 990-021) and added to an anhydrous, carefully weighed sample of unlabeled cholesterol to produce a stock of precisely determined specific activity. All three lipid stocks were stored under argon, in argon-saturated spectral chloroform, at −70 °C in the dark.

Vesicle Preparation. Large, multilamellar vesicles were prepared from quantitative mixtures of phosphatidylcholine and cholesterol stocks. Chloroform was removed under a stream of argon and then under high vacuum overnight. The dried sample, coated in a thin film on the wall of a round-bottom flask, was warmed to 30–35 °C (egg phosphatidylcholine) or 60 °C (DPPC), and an appropriate amount of aqueous 0.05 M KCl solution was added with vigorous vortexing for 1–2 min. The KCl solution was prepared from deionized, doubly glass-distilled, argon-saturated water and ultrapure KCl (Alfa-Ventron, Beverly, MA). The multilamellar vesicle suspensions were all adjusted to a final concentration of 0.5 mM (egg phosphatidylcholine) or 0.25 mM (DPPC) in total lipid. Suspensions were swirled gently for 2–6 h at 30–35 °C (egg phosphatidylcholine) or for 8–12 h at 60 °C (DPPC) before use. The exact lipid composition of the vesicle suspensions was determined by phosphate analysis (Chen et al., 1956) and ^{14}C scintillation counting. In all cases, the anticipated composition was within 2 mol % of the directly measured composition.

Small, unilamellar vesicles for DPH partitioning experiments were prepared by sonicating 1.0 mM lipid suspensions under argon in a small glass vial by means of a Heat Systems Ultrasonics W350 cell disruptor equipped with a titanium horn. Lipid suspensions were prepared directly in the glass vial used for sonication. Sonication temperatures were 50–56 °C for DPPC and 4–25 °C for egg phosphatidylcholine vesicles, depending on the cholesterol content. Sonicated suspensions were fractionated with respect to size by centrifuging at 168000*g* for 60 min, as described by Barenholz et al. (1977). Fractionated small vesicles were 0.4–0.7 mM in total lipid. Vesicles were stored under argon at 4–25 °C (egg phosphatidylcholine) or 60 °C (DPPC) for 8–12 h before use. As with multilamellar vesicles, directly determined compositions did not differ by more than 2 mol % from anticipated compositions.

Fluorescence Measurements. Zone-purified 1,6-diphenyl-1,3,5-hexatriene (DPH)[1] was obtained as a gift from Y. Barenholz and M. Shinitzky. DPH was introduced into vesicle suspensions by injection of an appropriate amount of a 10 mM DPH stock solution in tetrahydrofuran to give a final dye to lipid ratio of 1:500. Sufficient time for DPH incorporation was allowed in order to achieve an essentially steady level of fluorescence intensity, usually 2–8 h.

Details of the fluorescence measurements are described elsewhere (Shinitzky et al., 1971; Lentz et al., 1978), and we shall provide only a definition of the fluorescence-derived quantities used in this paper. The anisotropy of DPH fluorescence was taken as a measure of the rate and extent of hydrocarbon chain motion in the hydrophobic region of the bilayer, in accordance with the results and theory of Kawato

et al. (1977). The "microviscosity" was calculated from the anisotropy and the estimated fluorescence lifetime of DPH (Shinitzky et al., 1971; Lentz et al., 1976). As noted previously (Lentz et al., 1978), "microviscosity" need not be related to bulk viscosity but should be taken only as a convenient parameter describing DPH motion. The derivative of the natural logarithm of "microviscosity" with respect to reciprocal temperature is referred to as the "microviscosity activation energy" (Lentz et al., 1978) and is expected to be constant with temperature for a system not undergoing a phase separation or phase transition (Lentz et al., 1976). This quantity was obtained numerically by a stepwise quadratic fit of the microviscosity data. In variable-temperature experiments, DPH fluorescence anisotropy was recorded in both cooling and heating scans at scan rates of 18 °C/h using a T-system SLM 4000 fluorometer (SLM Instruments, Urbana, IL). Isothermal measurements were made after equilibration for 10 min at the desired temperature. The reproducibility of anisotropy measurements on turbid membrane suspensions was ±0.007.

Depolarization of DPH fluorescence due to light scattering was investigated by anisotropy measurements obtained with successively diluted samples (Lentz et al., 1979). Light-scattering depolarization must be distinguished from the fluorescence depolarization that results from DPH rotational motion. The latter depolarization is described here by the fluorescence anisotropy parameter. However, the directly measured anisotropy often reflects both motional and light-scattering depolarizations and must be corrected to obtain the value reflecting only probe rotational motion. The light-scattering depolarization correction term has been shown to be sensitive to membrane compositional and structural parameters (Lentz et al., 1979). Since the correction is necessitated by light scattering, it should reflect such parameters as vesicle size, shape, and refractive index. Fluorescence anisotropy values for DPPC–cholesterol large, multilamellar vesicles have been corrected for light-scattering depolarization. For all other membrane preparations, the magnitude of the light-scattering depolarization was insignificantly small.

Freeze–Fracture Electron Microscopy. Aliquots (1.0 mL) of DPPC–cholesterol multilamellar vesicle suspensions (0.5 mM) were equilibrated in plastic centrifuge tubes for at least 1 h at the temperatures from which freezing was desired. These samples were then pelleted in a Beckman Microfuge B equilibrated at roughly these temperatures. The pelleted vesicles were resuspended in about 0.05 mL of the supernatant and equilibrated for at least 48 h before freezing. Small portions of the samples were introduced by capillary action into a sandwich composed of a copper electron microscope grid (200 mesh, 0.01 mm) between two thin (0.1 mm) copper sheets (Mueller et al., 1980). The empty sandwiches were equilibrated on a brass block before addition of the sample. The added sample, sandwich and block were then further equilibrated in a closed, humidified chamber for 5 min (for samples to be frozen from above 40 °C), 7–8 min (30–40 °C), or 10–12 min (below 30 °C). The samples were very rapidly frozen by means of an automatic device that sprayed the sample with a blast of liquid propane precooled by liquid nitrogen according to Mueller et al. (1980). Through the use of very thin sandwiches (about 10 μm), freezing rates are achieved by this method which are comparable (Mueller et al., 1979) to rates achieved in other rapid freezing procedures (Ververgaert et al., 1973b; Gulik-Krzywicki & Costello, 1978). Such rapid freezing rates greatly reduce freezing artifacts such as reported by Costello & Gulik-Krzywicki (1976). Fracturing and platinum–carbon replication of the samples were carried out at −100 °C and 10^{-6} Torr in a Balzers BA360M freeze-etching apparatus equipped with electron guns. The sandwich was fractured by a mechanized force perpendicular to the sandwich plane. Replicas were floated on distilled water and cleaned in a 1:1 mixture of chloroform–methanol. Electron micrographs were taken on Kodak 4463 electron image film with a JEM 100 CX transmission electron microscope, operating at 80 kV.

Table I: Partition Coefficients for Distribution of DPH between Small Vesicles of Different Cholesterol Content

membrane A	membrane B	temp (°C)	$K_{A/B}$
egg PC	egg PC–25% cholesterol	15	1.05 ± 0.14
egg PC	egg PC–25% cholesterol	25	1.13 ± 0.20
egg PC	egg PC–33% cholesterol	15	0.86 ± 0.12
egg PC	egg PC–33% cholesterol	25	1.05 ± 0.10
egg PC	egg PC–50% cholesterol	15	0.52 ± 0.03
egg PC	egg PC–50% cholesterol	25	0.58 ± 0.09
egg PC	DPPC	28	0.85 ± 0.15
DPPC	DPPC–52% cholesterol	49	0.55 ± 0.07
DPPC	DPPC–34% cholesterol	49	0.53 ± 0.08
DPPC	DPPC–22% cholesterol	49	0.50 ± 0.08
DPPC	DPPC–16% cholesterol	49	0.66 ± 0.10
DPPC	DPPC–9% cholesterol	49	0.85 ± 0.09
DPPC	DPPC–9% cholesterol	43	1.01 ± 0.13

Results

Distribution of DPH between Vesicles of Different Cholesterol Content. The partition coefficients for DPH between small, unilamellar vesicles of differing cholesterol content were measured in order to test whether DPH could validly be used as a probe of "average" membrane structure in cholesterol–phosphatidylcholine membranes. [see Lentz et al. (1976) for derivation of the partition coefficient from anisotropy measurements.] Small, unilamellar vesicles were required for these studies since DPH exchange between large, multilamellar vesicles is too slow to reach equilibrium in a reasonable time (Lentz et al., 1976). The partition coefficients observed for distribution of DPH between pure phosphatidylcholine and cholesterol-containing vesicles are presented in Table I. These partition coefficients express the ratio of the equilibrium concentration of DPH in each of two accessible membrane environments. It is notable that the measured partition coefficients were for the most part close to 1.0 and in no instance less than 0.5 or greater than 2.0. According to the analysis of Sklar et al. (1979), partition coefficients within this range result in probe properties roughly reflecting the average of probe properties in the coexisting environments.

Fluorescence in DPPC–Cholesterol. The effective "microviscosities" derived from three typical cooling scans on DPPC–cholesterol multilamellar vesicles are presented as Arrhenius plots in Figure 1. A very dramatic change in the slope of these plots occurred at roughly 41 °C in pure DPPC and low cholesterol-containing vesicles. This dramatic change is associated with the main phase transition ($L\alpha \leftrightarrow P\beta'$). Subtle nonlinearities of these plots at somewhat lower temperatures are related to the pretransition ($P\beta' \leftrightarrow L\beta'$; Janiak et al., 1976) in pure DPPC bilayers. At high cholesterol contents (e.g., 31.5 mol % in Figure 1), no dramatic change was evident at temperatures near 41 °C. However, a clear change of slope occurred at roughly 35 °C. By analogy to microviscosity scans for mixtures of pure phospholipids (Lentz et al., 1976), this change in slope may be interpreted as reflecting the limit of a broad phase separation.

Changes in the temperature dependence of DPH motion are more easily detected in plots of the first derivative of

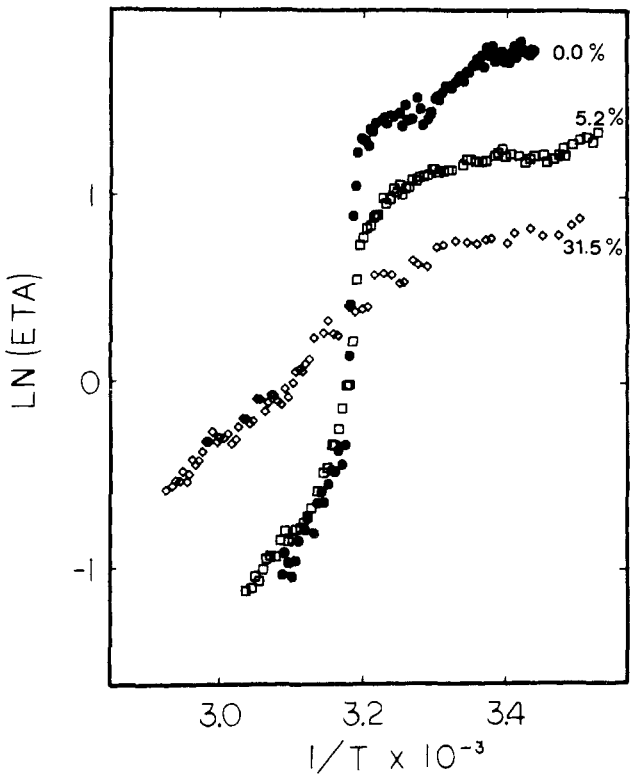

FIGURE 1: Representative Arrhenius plots of DPH-derived bilayer "microviscosity" (ETA) for large, multilamellar vesicles composed of DPPC and varying amounts of cholesterol. The data were generated at a scan rate of −18 °C/h. (●) Pure DPPC; (□) 5.2 mol % cholesterol–DPPC; (◇) 31.5 mol % cholesterol–DPPC.

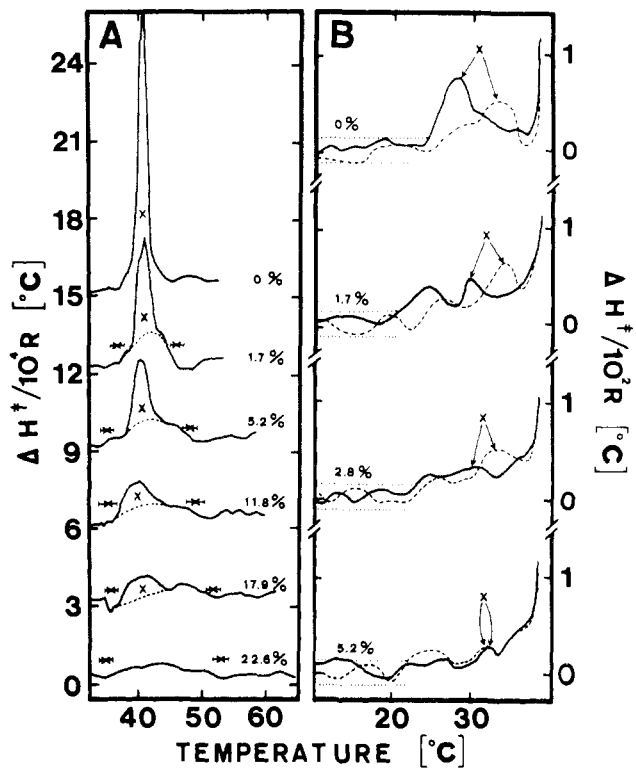

FIGURE 2: Temperature dependence of the DPH-derived "microviscosity activation energy" ($\Delta H^{\ddagger}$) for representative multilamellar vesicle samples composed of DPPC and the indicated mol % cholesterol. R is the universal gas constant. The data were generated at scan rates of ±18 °C/h. (A) Representative cooling scans shown through the "main" transition region. The curves are displaced on the ordinate by 15, 12, 9, 6, and 3 units for 0.0, 1.7, 5.2, 11.8, and 17.9 mol % cholesterol samples, respectively. For comparison with Figure 7A, peak positions are indicated by "X" and the delimiting temperatures of broad phase separations by "|—X—|" Our estimation of the broad peak in the main phase transition region is indicated by a dashed line. (B) Heating (- - -) and cooling (—) scans through the "pre" transition region for low-cholesterol-containing samples. The extent of fluctuations in the base line for pure DPPC is indicated (···). For comparison with Figure 7A, peak positions are indicated by "X".

"microviscosity", i.e., the "microviscosity activation energy". Data from several scans are plotted in this way in Figure 2. The cooling scans in Figure 2A show all the essential features of the main-phase transition in DPPC–cholesterol that have been reported calorimetrically (Estep et al., 1978; Mabrey et al., 1978). Thus, the introduction of cholesterol into DPPC vesicles resulted in the superposition of a broad peak on a sharp peak reminiscent of the sharp peak observed for pure DPPC. As shown in Figure 2A, the sharp peak persists clearly up to 11.8 mol % cholesterol and may be present in the 17.9 mol % cholesterol scan but is undetectable by 22.6 mol % cholesterol (Figure 2A). We have attributed the sharp peak to a phase transition analogous to that observed in pure DPPC. To indicate this, an "X" has been placed under each sharp peak in Figure 2A. On the other hand, the broad peak seemed most appropriately interpreted as indicative of a gradual phase separation and has been delimited by "|—X—|" in Figure 2A. Essentially identical results for the main-transition region were obtained in heating scans.

Figure 2B shows the microviscosity activation energy for heating and cooling scans through the pretransition region. In this region, a clear hysteresis was seen upon comparing heating and cooling scans. This has been previously reported for pure DPPC (Lentz et al., 1978). In the 1.7 mol % cholesterol sample, the pretransition is clearly identifiable but partially overlaps with an event at slightly lower temperature. This event is not evident in pure DPPC. At 2.8 mol % cholesterol, the pretransition is still identifiable. The lower temperature peak, however, is somewhat smaller. It is noteworthy that the extent of hysteresis in both the pretransition and the low-temperature event decreased with the addition of cholesterol. By 5.2 mol % cholesterol, the heating and cooling pretransition peaks are just visible above the range of low-temperature base-line fluctuations (··· in Figure 2B) and nearly overlap, indicating the disappearance of the hysteresis effect. The lower temperature event appears to be present but is not clearly resolved from the base-line. The disappearance of the pretransition at very low levels of cholesterol is consistent with previous descriptions of heating calorimetric results (Estep et al., 1978; Mabrey et al., 1978). The lower temperature event has not been reported before. It probably reflects increasing complexity of DPPC gel-phase behavior upon introduction of low concentrations of cholesterol.

The pretransition peak in heating and cooling scans is indicated by "X" in Figure 2B. Averaging the peak positions of heating and cooling scans yielded hysteresis-corrected pretransition temperatures of 31, 32, 31, and 32 °C for 0.0, 1.7, 2.8, and 5.2 mol % cholesterol, respectively. These are somewhat larger than, but in general compare well with, the previously reported value of 30 °C in pure DPPC (Lentz et al., 1978). The constancy of these values with increasing cholesterol content is noteworthy.

DPH fluorescence anisotropy was plotted as a function of membrane cholesterol content at three temperatures (Figure 3) to obtain more information on the location of phase boundaries. It was necessary to correct the observed anisotropies for depolarization due to scattering by the turbid membrane suspensions (Lentz et al., 1979). These light-scattering corrections are shown in Figure 4.

At 49 °C, the corrected anisotropy of DPH fluorescence

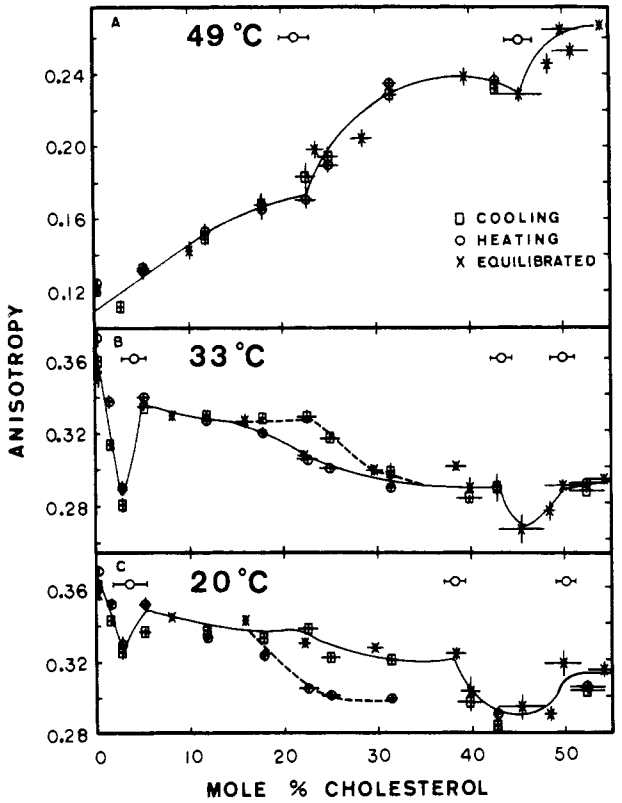

FIGURE 3: Dependence of DPH anisotropy (corrected for scattering-induced depolarization, see text) on cholesterol content in DPPC–cholesterol multilamellar vesicles. Horizontal and vertical lines through data points represent ±1 SD in composition and anisotropy, respectively. Data were obtained from cooling (□) and heating (○) scans at rates of ±18 °C/h or from 10-min equilibrations (X). Solid lines are drawn through the data obtained from scanning and equilibration experiments when these agreed. Dashed lines are drawn through scanning results that were in disagreement with equilibrated measurements. Symbols (|—○—|) drawn over the data indicate regions of inflection. Data obtained at (A) 49, (B) 33, and (C) 20 °C.

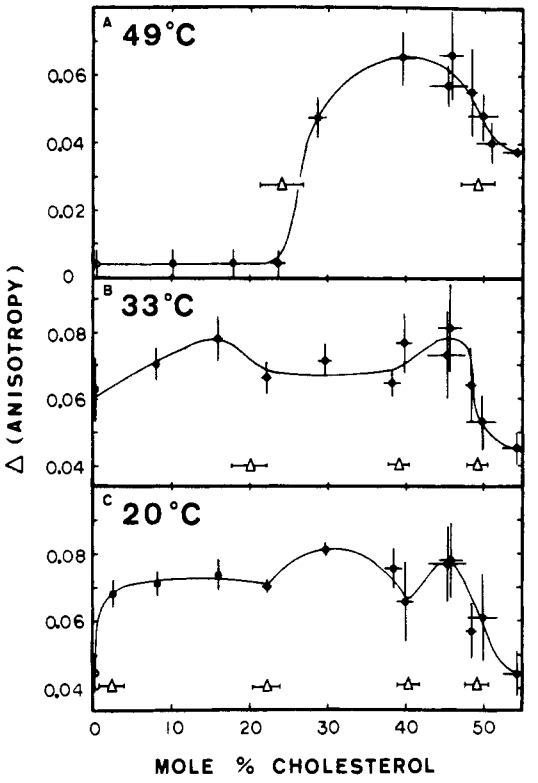

FIGURE 4: Correction to the observed DPH fluorescence anisotropy necessitated by light scattering of 0.5 mM DPPC–cholesterol multilamellar vesicle suspensions as a function of cholesterol content. Error bars represent ±1 SD in composition and anisotropy correction. Symbols (|—Δ—|) indicate regions of inflection, as in Figure 3. Data obtained at (A) 49, (B) 33, and (C) 20 °C.

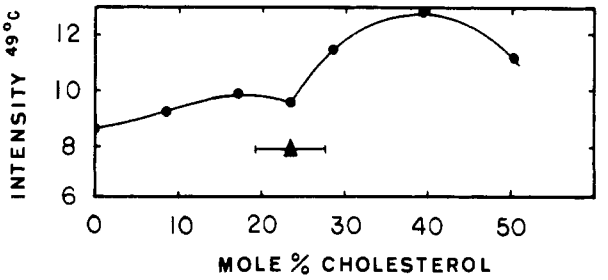

FIGURE 5: Relative intensity of DPH fluorescence (in arbitrary units) at 49 °C in DPPC–cholesterol multilamellar vesicles as a function of cholesterol content. A region of inflection occurs at about 22 mol % cholesterol, as indicated by a horizontal symbol (|—▲—|).

was observed generally to increase with cholesterol content (Figure 3A). However, the data deviated significantly from a simple monotonic behavior. Consequently, the data were best fit by a curve showing distinct inflections at 20 and 46 mol % cholesterol (Figure 3A). These inflections are even more dramatically evident in the measured light-scattering depolarization corrections at 49 °C (Figure 4A). The depolarization correction was found to be insignificant at low cholesterol content, increased dramatically at about 20 mol % cholesterol, and then decreased sharply between 45 and 50 mol % cholesterol. Taken together, Figures 3A and 4A suggest a membrane structural variation at 49 °C over the range of 20–48 mol % cholesterol. This variation in structure only slightly altered acyl-chain motion within the bilayer but changed the light-scattering properties of the vesicles dramatically.

At 33 and 20 °C, the variation of DPH fluorescence anisotropy with cholesterol content was more complex than at 49 °C. First, the 33 and 20 °C anisotropy isotherms show near discontinuities at roughly 3–6 mol % cholesterol, with the dip at 33 °C (Figure 3B) being more dramatic than that observed at 20 °C (Figure 3C). Second, dramatic history-dependent behavior is observed in the range of roughly 20–30 mol % cholesterol at both 33 and 20 °C (Figure 3B,C). This history dependence is probably indicative of complex structural changes occurring in this region. It also prevents the precise determination of compositional boundaries through this region.

Finally, clear inflections are observed in the anisotropy data at roughly 40 and 50 mol % cholesterol (Figure 3B,C). These inflections are substantiated by similar events seen in the light-scattering depolarization correction isotherms (Figure 4B,C). These and other composition ranges corresponding to discontinuities or inflections have been indicated in Figures 3 and 4 by "|—○—|" and "|—Δ—|", respectively. They will be discussed in terms of the positions of phase boundaries (see Discussion).

To further define the behavior of DPH in cholesterol–DPPC multilamellar vesicles, we have measured the variation of relative fluorescence intensity with cholesterol content at 49 °C (Figure 5). Clear trends in fluorescence intensity with cholesterol content were not observed at low temperature. In agreement with the anisotropy (Figure 3A) and the depolarization correction (Figure 4A) data, the intensity showed an inflection at roughly 22 mol % cholesterol. This suggests a change in the DPH microenvironment at this cholesterol concentration. The coordinates of inflections and peaks ob-

served in plots such as those shown in Figures 1–5 have been summarized in the temperature–composition diagram shown in Figure 7A.

Freeze–Fracture of DPPC–Cholesterol. Freeze–fracture electron microscopy was used to test for single or coexisting fracture-face morphologies in samples of different compositions which were rapidly frozen from several temperatures. The morphologies of many of the membrane fracture faces were quite complex as illustrated by the representative micrographs presented in Figure 6. We have attempted to simplify our observations by characterizing the observed morphologies in terms of five essential structures: planar (P), rivuletted (R), banded (B), jumbled (J), and mottled (M). Examples of planar and rivuletted structures are shown in Figure 6G and in the lower half of Figure 6A, respectively. The banded morphology consists of closely spaced (upper half of Figure 6A) or widely spaced (seen faintly in Figure 6E) parallel bands. Bands are distinguished from rivulettes by the greater apparent depth of the rivuletted structure (compare lower and upper portions of Figure 6A). Jumbled morphologies appear to contain many disoriented, irregular, small rivulettes, as reported previously [Figures 2A and 3A of Luna & McConnell (1977); Figure 6A of Gulik-Krzywicki & Costello (1978)]. Extremely irregular structures showing no repeatable pattern are referred to as "mottled". Mottled regions may be observed coexisting with rivuletted ones in Figure 6C, and mottled morphology with a hint of banding (M/B) may be seen coexisting with planar regions in Figure 6B.

As may be seen in Figure 6B–D,F,H, two distinct structures were often observed to coexist within the same fracture face. Such instances have been described by indicating the two coexisting structures as follows: M/B,P (Figure 6B); R,M (Figure 6C); R,P (Figure 6D); P,P′ (Figure 6F,H). In the last instance, similar planar structures are visible, but on different levels. This situation is easily distinguishable from two planar fracture faces, which are separated by a more clearly defined ridge (e.g., see Figure 6E–H).

In Figure 7C, we have summarized our freeze–fracture observations on a temperature–composition diagram. Single letters indicate the observation of a single fracture-face morphology in samples frozen from the plotted temperature. Composition–temperature conditions resulting in coexisting morphologies are indicated by two letters separated by a comma (e.g., P,R or P,P′).

Egg Phosphatidylcholine–Cholesterol Vesicles. The anisotropy of DPH fluorescence is plotted in Figure 8 as a function of cholesterol content in egg phosphatidylcholine–cholesterol vesicles. At each of the three temperatures examined, these data were best fit in three segments. At each temperature, the individual segments are seen to join at points where the first derivative is discontinuous. One discontinuity occurs at 17 and the other at 33–36 mol % cholesterol. These plots should be compared to the analogous one for DPPC–cholesterol at 49 °C (Figure 3A). Two similarities between egg phosphatidylcholine (15–37 °C) and DPPC (49 °C) data are evident. First, the DPH anisotropy was best fit by three negatively curved segments. Second, the anisotropy generally increased with increasing cholesterol in both cases. By contrast to the behavior of DPPC–cholesterol multilamellar vesicles, however, corrections to the observed anisotropy due to light scattering were insignificant for all mixtures of egg phosphatidylcholine–cholesterol studied.

Discussion

DPH as a Probe in Cholesterol-Containing Membranes. DPH fluorescence provides a rapid, sensitive, and easily interpretable measure of changes in membrane structure (Lentz et al., 1976, 1978). Nonetheless, as with all probe techniques, care must be taken in its application. Interpretation of data from DPH in cholesterol–phosphatidylcholine membranes requires that we establish (a) the location of the probe in the membrane, (b) what aspect of the membrane molecular structure is reflected in the measured probe property, and (c) the degree to which the probe perturbs the membrane structure.

First, with regard to location within the membrane, two studies have indicated that DPH probably intercalates between the acyl chains of a pure phospholipid bilayer (Andrich & Vanderkooi, 1976; Kawato et al., 1977). Other studies have shown DPH to partition roughly equally between gel phase and liquid-crystalline phase bilayers (Lentz et al., 1976). Our results (Table I) further suggest that DPH does not partition strongly in favor of saturated or unsaturated, gel or liquid crystalline, or cholesterol-rich vs. cholesterol-free membranes. Thus, the measured DPH anisotropy should reflect the average structure of the different domains within a bilayer.

Second, recent time-resolved measurements (Kawato et al., 1978) have extended to DPPC–cholesterol bilayers the model for DPH motion proposed for pure DPPC. In this model, DPH fluorescence anisotropy reflects the extent of acyl-chain motion within the bilayer. Thus, DPH anisotropy should be directly related to an acyl-chain order parameter (Kawato et al., 1977) and inversely proportional to the average number of gauche conformations per acyl chain. In this regard, we have observed increasing cholesterol to have generally opposite effects on DPH anisotropy above and below the DPPC phase transition (Figure 3). A similar effect has been observed for the number of acyl-chain gauche conformations by Raman spectroscopy (Lippert & Peticolas, 1971) and for the acyl-chain order parameter reported by a deuterated phospholipid probe (Jacobs & Oldfield, 1979). This parallel between Raman, deuterium magnetic resonance, and fluorescence results further supports the proposed model for DPH motion in the bilayer.

Finally, the agreement of our results (e.g., Figure 2) with microcalorimetric data (Estep et al., 1978; Mabrey et al., 1978) confirms the ability of DPH anisotropy measurements to reflect phase changes in cholesterol-containing membranes. These results extend to DPPC–cholesterol vesicles our previous conclusions that DPH produces only minor perturbations on the phase transition of phospholipid vesicles (Lentz et al., 1978).

DPPC–Cholesterol Phase Diagram. We interpret inflections and discontinuities in DPH fluorescence properties (shown in Figures 1–5) as indicative of DPPC–cholesterol phase behavior. Specifically, we assume that the temperatures and compositions at which these events occur should fall on the phase boundaries of the DPPC–cholesterol phase diagram. With this assumption, we have plotted the coordinates of peaks (X in Figure 2), broad event delimitations, (|—X—| in Figure 2), and isothermal inflections (|—○—|, |—△—|, and |—▲—| in Figures 3, 4, and 5, respectively) in a temperature–composition diagram (Figure 7A). In addition, the appearance of one or two morphologies in our freeze–fracture replicas is indicated in Figure 7C. A consistent interpretation of both our fluorescence and freeze–fracture data is provided by the phase diagram shown in Figure 7C.

An assumption crucial to the construction of the phase diagram in Figure 7 is the applicability of the phase rule to multilamellar vesicle membranes. The phase rule is applicable to isothermal phase equilibria in macroscopic (i.e., thermo-

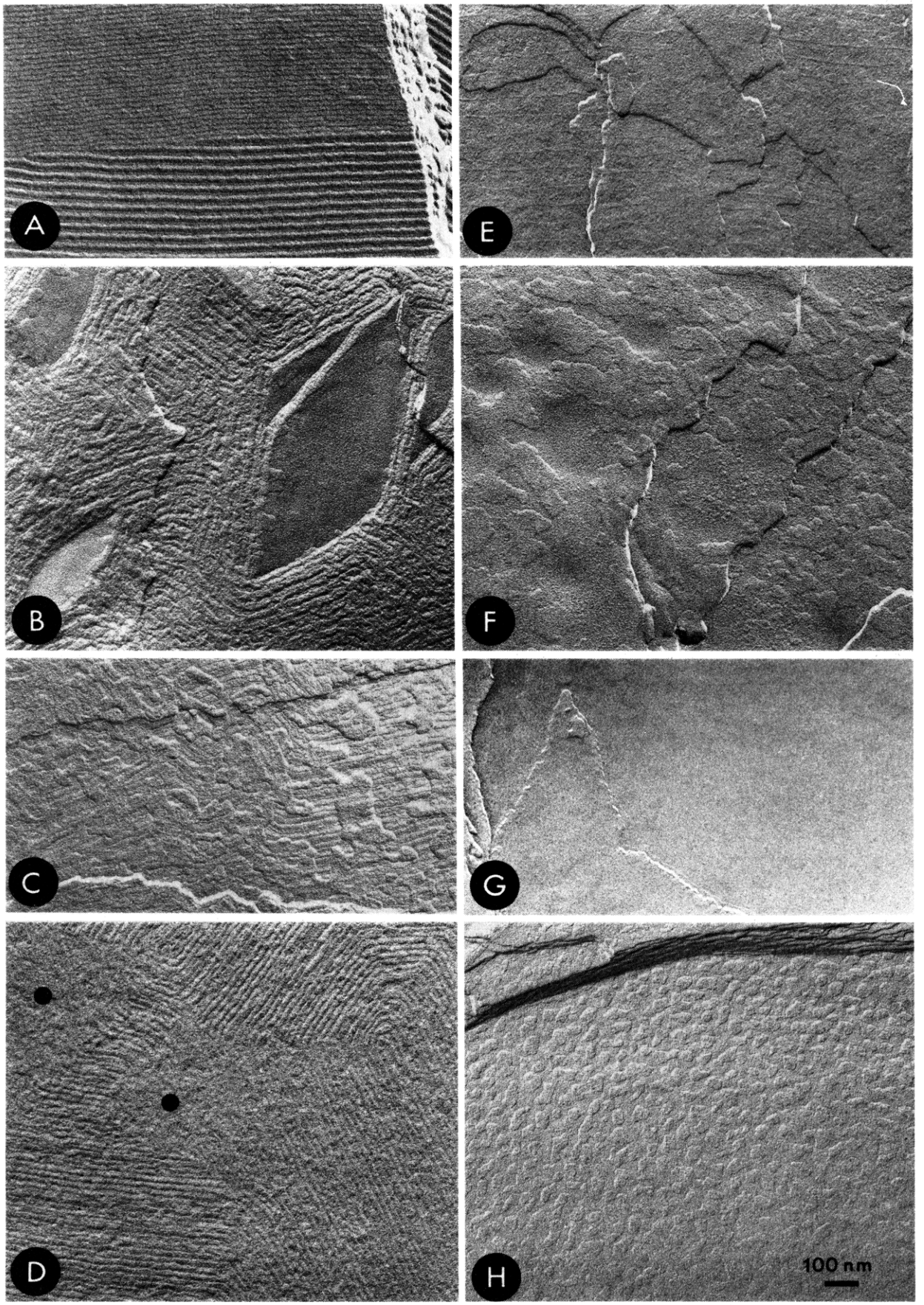

FIGURE 6: Electron micrographs of freeze–fracture replicas prepared from DPPC–cholesterol multilamellar vesicles and quenched from several temperatures. Platinum shading was from below, at an angle of 45° from the specimen platform. Magnification 58 125×. (A) 3.4 mol % cholesterol frozen from 34.5 °C; (B) 6.9 mol % cholesterol from 24 °C; (C) 6.3 mol % cholesterol from 31.5 °C; (D) 6.9 mol % cholesterol from 39.5 °C; (E) 13.3 mol % cholesterol from 20 °C; (F) 24.3 mol % cholesterol from 24 °C; (G) 29.3 mol % cholesterol from 39 °C; (H) 29.3 mol % cholesterol from 44 °C.

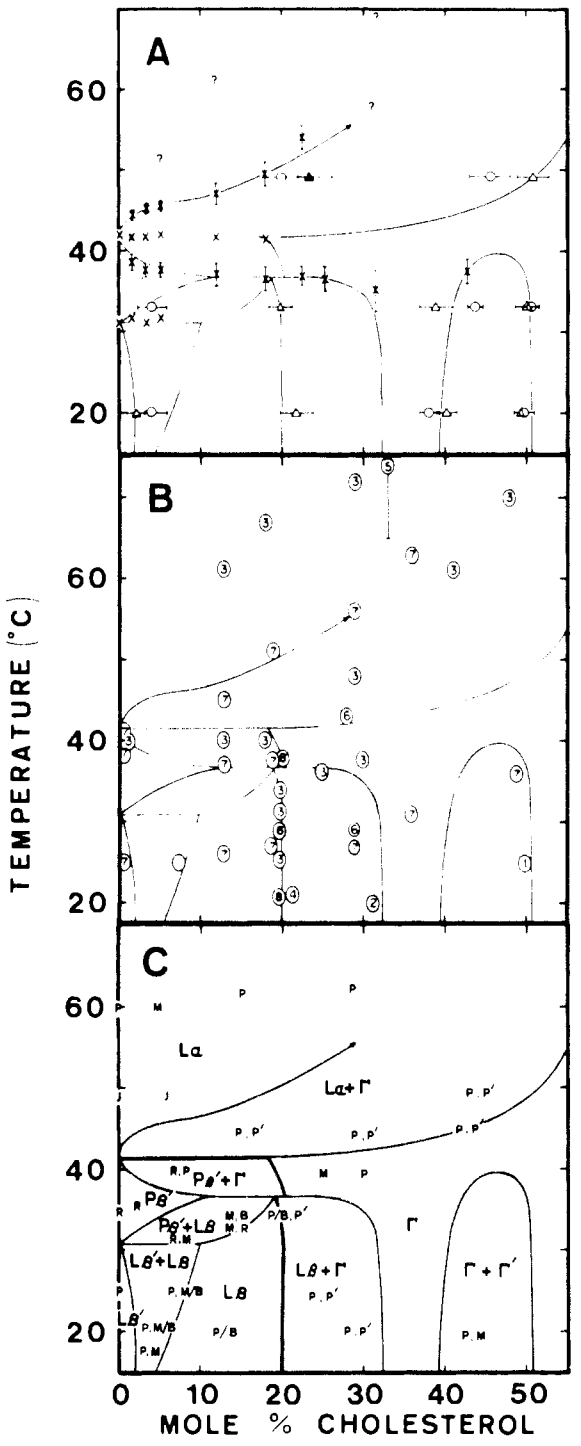

FIGURE 7: Temperature–composition diagram for multilamellar vesicles containing DPPC and cholesterol. (A) Experimental data: (⊼) delimiting temperatures of broad changes detected in microviscosity Arrhenius plots (such as shown in Figure 1) and/or in microviscosity activation energy plots (such as shown in Figure 2); (X) peak temperatures of sharp changes detected in microviscosity activation energy plots; (|—○—|) inflections in anisotropy isotherms (Figure 3); (|—△—|) inflections in anisotropy scattering correction isotherms (Figure 4); (|—▲—|) inflection in both anisotropy scattering correction (Figure 4) and fluorescence intensity isotherms (Figure 5). Error bars represent estimated uncertainty and include such factors as agreement of heating and cooling scans, errors inherent in estimating inflection points, and known errors in temperature and composition measurements. (B) Compilation of literature data compared to our proposed phase diagram. The numbers refer to entries in Table II. (C) Summary of freeze–fracture electron microscopy results together with phase assignments. Observed morphologies are indicated by P, planar; M, mottled; R, rivuletted; B, banded; and J, jumbled. Proposed phase assignments[2] are shown in large letters.

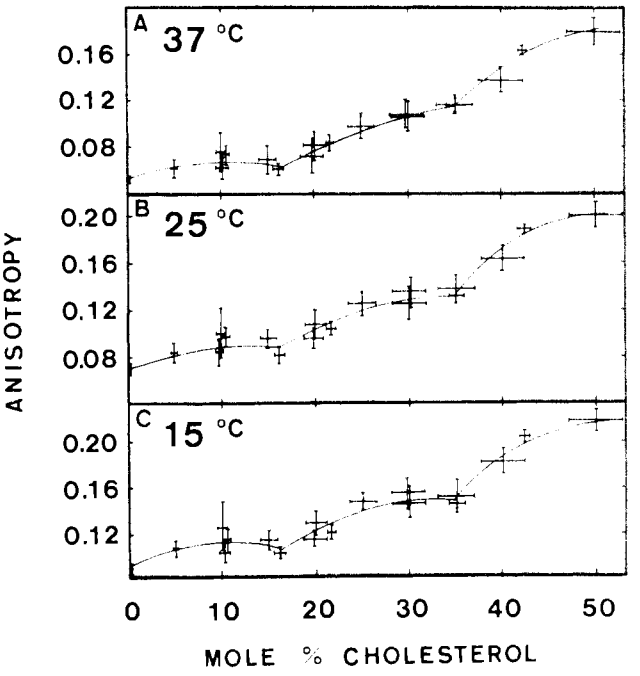

FIGURE 8: Dependence of DPH anisotropy on cholesterol content in egg phosphatidylcholine–cholesterol multilamellar vesicles. Error bars represent ±1 SD in composition and anisotropy. The curves are our interpretation of best fits to the data. Data obtained at (A) 37, (B) 25, and (C) 15 °C.

dynamic) systems. Although these membrane systems are small, they contain a sufficiently large number of molecules to be treated in the thermodynamic limit. Recent calorimetric studies of the main phase transition in multilamellar vesicles prepared from highly purified DPPC have suggested that this transition is isothermal and first order (Albon & Sturtevant, 1978) and thus support our application of the phase rule. Consistent with this approach and with the suggestion of Mabrey & Sturtevant (1976), we have ignored the breadth of the pure DPPC transitions in constructing our phase diagram. In interpreting our results, we have also insisted that the proposed phase diagram obey the boundary and boundary–curvature rules of phase diagram construction (Gordon, 1968) and that it be consistent with the known phase behavior of pure DPPC (Janiak et al., 1976). These requirements, along with the phase rule itself, set severe limitations on the ways in which the phase diagram can be drawn consistent with our data. Although the detailed positions of some lines remain uncertain, the general features of the diagram in Figure 7C are required in order to satisfy all these constraints.

The positions of most of the phase lines have been estimated from our fluorescence data, as summarized in Figure 7A. The specific lamellar phase structures proposed for different regions of this phase diagram (Figure 7C) were assigned on the basis of literature reports and thermodynamic rules. The assignment of $L\alpha$, $P\beta'$, and $L\beta'$ phases[2] along the temperature axis was on the basis of the reported phase structure of pure DPPC (Janiak et al., 1976).[3] Since we had no clear evidence for

[2] Lipid phase nomenclature [after Tardieu et al. (1973) except for Γ]: $L\alpha$, lamellar, disordered acyl chains; $L\beta$, lamellar, acyl chains extended parallel to the bilayer normal; $L\beta'$, lamellar, acyl chains extended at an acute angle to the bilayer normal; $P\beta'$, pleated, acyl chains extended at an acute angle to the bilayer normal; Γ, unknown structure occurring at high cholesterol content.

Table II: Summary of Literature Results Indicative of DPPC–Cholesterol Phase Boundaries

points in Figure 7B	observable	X_{choles}	nature of evidence	temp (°C)	ref
1	X-ray diffraction pattern	0.075	max in the small-angle spacings with no significant change in large-angle spacings	25	Ladbrooke et al. (1968)
		0.50	appearance of pure cholesterol spacings with increase in cholesterol	25	
2	X-ray diffraction pattern	0.315 ± 0.15	sharp 4.2-A large-angle spacing disappeared with increased cholesterol, leaving broad 4.7-A spacing	20	Engelman & Rothman (1972)
3	spin-labeled phosphatidylcholine order parameter	0.2 0.2 0.22 0.30	inflection point[a] in graph of order parameter vs. cholesterol content	25.5 30.5 34.0 37.5	Shimshick & McConnell (1973)
	Tempo water–lipid partition coeff	see Figure 7B	nonlinearities or inflections in temperature scans	see Figure 7B	
4	order parameter for 5-doxyl- and 12-doxylstearic acid	0.215 ± 0.015	discontinuity in the order parameter behavior with increased cholesterol	21.5 ± 1.5	Schreier-Muccillo et al. (1973)
5	NMR spectrum of [4-^{13}C] cholesterol	0.33	appearance of two peaks upon lowering temperature	65–82	Opella et al. (1976)
6	^{2}H NMR spectrum of DPPC containing labeled fatty acids	0.20 0.29	disappearance of signals from the two fatty acid chains with decreased cholesterol	29	Haberkorn et al. (1977)
		0.28	inflection in quadrupole coupling with change in cholesterol	43	
7	fluorescence intensity of chlorophyll *a* in membranes	see Figure 7B	nonlinearities or inflections in temperature scans	see Figure 7B	Lee (1976)
8	lateral diffusion of fluorescent lipid probe	0.2 0.2	sudden increase in diffusion coeff with increased cholesterol	21 38	Rubenstein et al. (1979)

[a] Taken from Figure 4 of Shimshick & McConnell (1973).

a phase line above the liquidus line (the $L\alpha \leftrightarrow L\alpha + \Gamma$ boundary in Figure 7C), the entire region above this boundary has been designated "Lα". Below the main phase separation region, our fluorescence results suggested several phase lines. Ladbrooke et al. (1968) reported an Lβ-like phase at 25 °C at greater than about 7.5 mol % cholesterol. We have made our assignment of the Lβ phase in Figure 7C on the basis of this report. The two-phase regions between Lβ' and Lβ and between Pβ' and Lβ were suggested by both our freeze–fracture and fluorescence data and required by the phase rule.

At high cholesterol content, our interpretation predicts a phase of unknown structure, designated in Figure 7C as "Γ". Although the detailed molecular structure of this phase cannot be determined from our data, some indication of its nature can be gleaned. First, we note that the inflection in DPH fluorescence anisotropy across the $L\alpha \leftrightarrow L\alpha + \Gamma$ phase line (20 mol % inflection in Figure 3A) was less dramatic than that observed across many other phase boundaries. This suggests that DPH motion within the Γ phase may be similar to that within the Lα phase at high cholesterol content. Clearly, however, there are differences in packing or gross membrane structure as indicated by the dramatic change in light-scattering properties evident in Figure 4A. Second, the decrease of DPH fluorescence anisotropy with cholesterol content at low temperatures (Figure 3) indicates the increased extent of DPH motion in the Γ phase relative to the Lβ phase. Indeed, the gel-phase miscibility gap shown in our proposed phase diagram ($L\beta + \Gamma$ region in Figure 7C) would suggest very different structures for the Lβ and Γ phases (Gordon, 1968). Finally, the large-angle X-ray diffraction band from DPPC–cholesterol multilayers containing greater than 30 mol % cholesterol at 20 °C is reported to be broad and liquid-like with a peak near 4.7 Å (Engelman & Rothman, 1972). Taking all this information together, Γ must be a phase considerably disordered in local molecular packing by the presence of cholesterol. A similar phase of slightly different structure (Γ') was implied by our data at even higher cholesterol concentration (see the $\Gamma + \Gamma'$ two-phase region in Figure 7C).

Our fluorescence data detect ten of the phase boundaries shown in Figure 7C. The remaining five boundaries, however, have been difficult to define solely on the basis of fluorescence data. In these instances, we have taken advantage of our freeze–fracture results, relevant literature reports, and the requirements of the phase rule. The first two phase boundaries falling into this category are those defining the $P\beta' + L\beta \leftrightarrow L\beta$ and $L\beta' + L\beta \leftrightarrow L\beta$ equilibria. They are required by our freeze–fracture data and supported by the observation of Ladbrooke et al. (1968) (see point "1" in Figure 7B and Table II). In addition, the phase rule requires that the $P\beta' + L\beta \leftrightarrow L\beta$ boundary join the horizontal $P\beta' + \Gamma \leftrightarrow P\beta' + L\beta$ line and the $L\beta + \Gamma \leftrightarrow L\beta$ line in a triple point, as shown. The suggestion of such a triple point has been made previously by Shimshick & McConnell (1973). The third phase boundary falling into this uncertain category is the short segment defining the $P\beta' + \Gamma \leftrightarrow \Gamma$ equilibrium. This line is implied by our freeze–fracture results and is necessary to explain the

[3] A reviewer has correctly pointed out that the shape of the proposed phase diagram (Figure 7) violates the rules of phase diagram construction. Specifically, at a very low mole fraction of cholesterol, the diagram is drawn intersecting the pure DPPC axis in a way inconsistent with the boundary–curvature rule (Gordon, 1968). This problem can be avoided by insertion of proper triple points at very low cholesterol content. Unfortunately, neither our data nor data in the literature can establish the exact nature of these triple points (probably eutectic near the main transition and peritectic near the pretransition). Because of this uncertainty and our inability to define the nature of very low cholesterol samples, we have chosen to present our proposed phase diagram in the simplified manner shown.

superimposed sharp and broad "main" phase transitions (Figure 2A). In our interpretation, the broad change corresponds to the gradual separation of the Γ from the $L\alpha$ phase or the $P\beta'$ from the Γ phase. The sharp transition is explained by an $L\alpha + \Gamma \rightarrow P\beta' + \Gamma$ phase change which should be essentially identical with the main ($L\alpha \rightarrow P\beta'$; Janiak et al., 1976) transition observed in pure DPPC. In the context of this interpretation, the position of the $P\beta' + \Gamma \leftrightarrow \Gamma$ boundary predicts the observed disappearance of the sharp peak at about 20 mol % cholesterol (Figure 2A; Estep et al., 1978; Mabrey et al., 1978). The fourth phase boundary requiring discussion is the $L\beta + \Gamma \rightarrow \Gamma$ line whose horizontal portion is suggested by our fluorescence data. The nearly vertical portion of this boundary, however (at roughly 33 mol % cholesterol), has been defined mainly on the basis of two literature reports (Engelman & Rothman, 1972; Haberkorn et al., 1977; points "2" and "6" of Figure 7B; cf. Table II). The study of Engelman & Rothman is especially significant since it reported the disappearance of large-angle X-ray diffraction spacings characteristic of an $L\beta$-type phase. The fifth poorly defined boundary is that corresponding to the $L\alpha + \Gamma \leftrightarrow \Gamma$ change. This line is supported by one fluorescence data point at roughly 50 mol % cholesterol, by our freeze–fracture results and by the deuterium nuclear magnetic resonance data of Haberkorn et al. (1977) ("6" in Figure 7B and Table II). Our previous remarks about the similarity of the $L\alpha$ and Γ phases make the difficulty in detecting this line understandable.

The electron micrographs shown in Figure 6 provide further support for the phase assignments made in Figure 7. Regions interpreted in Figure 7C as supporting two coexisting phases yielded samples that showed coexisting morphologies upon freeze–fracture. Thus, the smooth, diamond-shaped domains found in the $L\beta + L\beta'$ region were always surrounded by a mottled or lightly banded morphology. Our interpretation is that this mottled morphology reflects the inability of cholesterol to intercalate into the tilted $L\beta'$ phase. The smooth (diamond-shaped) areas presumably reflect the successful intercalation of cholesterol into the $L\beta$ phase. The well-defined shape of these areas is interesting. Gebhardt et al. (1977) have predicted that coexisting "crystalline" phases of different symmetry would produce such roughly geometric patterns when forced to pack together in a bilayer. Similarly, roughly diamond-shaped, mottled regions (indicated by ●) can be seen in the midst of rivuletted morphology in Figure 6D. These characterize samples quenched from the $P\beta' + \Gamma$ portion of the phase diagram. Interestingly, samples frozen from the $P\beta' + L\beta$ region did not show such regular, geometric domains (Figure C). In other two-phase regions of the phase diagram, regions of nondescript shape could be seen superimposed on a planar background. This was especially evident in the "pebble beach" pattern seen in the $L\alpha + \Gamma$ region (Figure 6H) but could also be seen in the $L\beta + \Gamma$ (Figure 6F) and $\Gamma + \Gamma'$ (not shown) regions. Such patterns have been discussed in theory for coexisting phases whose symmetries might be more compatible (Gebhardt et al., 1977).

Samples quenched from conditions expected to support only a single phase produced freeze–fracture replicas showing only one morphology, as in Figure 6E,G, representing $L\beta$ and Γ phases, respectively. Replicas of samples quenched from other single-phase regions (i.e., $L\alpha$ and $L\beta'$) showed morphologies that have been previously reported (Luna & McConnell, 1977; Ververgaert et al., 1973a). It is worth noting here that indistinct banding patterns were often superimposed on a planar or mottled morphology in low-cholesterol-containing samples frozen from around 20 °C. This is illustrated in Figure 6E. When short equilibration times (1–2 h) were used before freezing, we observed clearly rivuletted or banded morphologies in such samples. These observations explain the reports of $P\beta'$ morphologies at temperatures well below those expected to support the $P\beta'$ phase (Ververgaert et al., 1973a; Verkleij et al., 1974). Presumably, these results reflect difficulty in annealing out the $P\beta'$ structure. In this context, the history-dependent morphology observed below the main transition of pure DPPC (Luna & McConnell, 1977) can be understood.

Comparison with Previously Proposed DPPC–Cholesterol Phase Diagrams. Several attempts at defining the phase diagram for DPPC–cholesterol mixtures have been made. The first such diagram was reported by Shimshick & McConnell (1973) on the basis of electron spin resonance probe studies. The boundary coordinates from this study are shown in Figure 7B as "3". The boundary of the Shimshick and McConnell phase diagram that defines the $L\alpha + \Gamma \leftrightarrow L\alpha$ equilibrium is in disagreement with our results. This boundary in Shimshick and McConnell's study was defined by Tempo[1] partitioning data. It may be that Tempo partitioning is more sensitive to the formation of Γ phase than is DPH fluorescence anisotropy. In this regard, Mabrey et al. (1978) reported heat capacity profiles for DPPC–cholesterol vesicles that were somewhat broader than the DPH microviscosity activation energy profiles we have observed (Figure 2A), while Estep et al. (1978) showed heat capacity profiles that were in agreement with our results. Germane to this issue, we have occasionally observed peaks in our microviscosity activation energy profiles at temperatures above the liquidus line in Figure 7C. The upper delimiting temperatures of these peaks were not well-defined but have been indicated in Figure 7A by "?". It may be, therefore, that the phase structure of the $L\alpha$ region is more complex than we have indicated. Since our data are incapable of resolving this issue, we have made in Figure 7C the simplest possible interpretation. In addition to the $L\alpha + \Gamma \leftrightarrow L\alpha$ phase line, we disagree with Shimshick and McConnell on the position of the $L\alpha + \Gamma \leftrightarrow \Gamma$ boundary. The Shimshick and McConnell data correspond more to the midpoint of the $L\alpha + \Gamma$ region in our interpretation. No obvious explanation presents itself. On two other boundaries of the phase diagram ($L\alpha + \Gamma \leftrightarrow P\beta' + \Gamma$, $L\beta \leftrightarrow L\beta + \Gamma$), our results are in agreement with Shimshick and McConnell (see Figure 7B and Table II).

Lee (1976) has proposed a phase diagram for multilamellar dispersions of DPPC and cholesterol on the basis of changes in fluorescence intensity of chlorophyll *a* incorporated into the bilayer. Lee's boundary coordinates are plotted as "7" in Figure 7B (Table II). They agree with ours in identifying the $L\alpha \leftrightarrow L\alpha + \Gamma$ and $P\beta' + \Gamma \leftrightarrow P\beta' + L\beta$ boundary lines. Other data points from Lee's study generally follow our phase lines, although this may be fortuitous since many of Lee's points fall near essentially vertical boundaries that should not have been detectable by his temperature-scanning experiments.

Finally, Rubenstein et al. (1979) have recently reported the temperature and cholesterol content dependence of lipid lateral diffusion coefficients in DPPC–cholesterol oriented multilayers. These authors reported dramatic changes in diffusion coefficients at 20 mol % cholesterol at two temperatures. These inflections are indicated by "8" in Figure 7B. Rubenstein et al. also presented a much more complete study of dimyristoylphosphatidylcholine–cholesterol bilayers and interpreted their results in terms of a temperature–composition diagram. This diagram defined the boundary between regions of slow and fast lateral diffusion. We can extrapolate this diagram to our DPPC–cholesterol diagram. If we do so, this

boundary would roughly correspond to the thickly drawn phase lines of Figure 7C. These phase boundaries separate gel-like phases ($P\beta'$, $L\beta'$, $L\beta$) from liquid-crystalline phases and the presumably isomorphous Γ phase. Since lipid lateral diffusion has been observed to be much slower in the gel phases than in the liquid-crystalline phase (Fahey & Webb, 1978), the results of Rubenstein et al. are completely consistent with our phase diagram.

A number of investigations of DPPC–cholesterol have been published but not interpreted in terms of a phase diagram. We have summarized in Table II those studies that we feel provide evidence for phase lines. The points implied by these reports are indicated in Figure 7B. It is clear from Figure 7B and Table II that our proposed phase diagram offers an explanation for most of these reports. It should be noted that the observation of Opella et al. (1976) ("5" in Figure 7B) is more in accord with the liquidus line of Shimshick and McConnell than with Lee's or our results. Also, Ladbrooke et al. (1968) suggested the existence of pure cholesterol domains above 50 mol % cholesterol ("1" in Figure 7B). While our phase diagram does not predict pure cholesterol domains, it may be that a narrow Γ' region occurs just above 50 mol % cholesterol, followed by a two-phase region with one phase being cholesterol. Alternatively, the diffraction pattern observed by Ladbrooke et al. may have been that of Γ' phase rather than that of neat cholesterol.

$P\beta'$ Banding Patterns. The rivuletted structure commonly associated with the $P\beta'$ phase (Tardieu et al., 1973; Ververgaert et al., 1973a; Luna & McConnell, 1977) was superimposed in our micrographs with a "banding" which is discernible between peaks of the rivulettes (Figure 6A). Under different shading conditions (not shown), similar bands were observed at the peaks of rivulettes. A similar pattern was shown but not noted by Luna & McConnell (1977) for pure DPPC.

It is also notable that the rivuletted pattern was found in the same sample with a purely banded pattern of different periodicity, even in pure DPPC. Figure 6A illustrates this. Such variability in $P\beta'$ periodicity has been previously noted (Ververgaert et al., 1973a). The coexistence of two structures in the $P\beta'$ region requires special comment. Certainly, a single-component system (pure DPPC) cannot support two coexisting phases at the same temperature and pressure, as our results suggest. The fallacy here is that we are actually dealing with an additional component. The component that is generally ignored in the construction of membrane phase diagrams is water (Shimshick & McConnell, 1973; Lentz et al., 1976; Mabrey & Sturtevant, 1976). For lamellar phases (i.e., $L\alpha$, $L\beta$, $L\beta'$), variations in water content produce only slight variations in the bilayer thickness (maximum to 5 Å for $L\beta'$ phase, Tardieu et al., 1973) and therefore should not be detectable in freeze–fracture. Our observed morphologies for the $L\alpha$ and $L\beta'$ phases support this contention. However, the two-dimensional $P\beta'$ lattice symmetry (Tardieu et al., 1973) sensitively links the undulation periodicity, the chain tilt angle, and the undulation amplitude with the interbilayer water content (Janiak et al., 1976). It seems likely, therefore, that the two morphologies seen in Figure 6A represent $P\beta'$ structures of slightly different water content and consequently different undulation amplitudes and periodicities. Such differences in amplitude and periodicity can completely explain the two observed $P\beta'$ morphologies, if we adopt the view of $P\beta'$ structure espoused by Gebhardt et al. (1977).

Comparison of DPPC–Cholesterol and Egg Phosphatidylcholine–Cholesterol Multilamellar Vesicles. The phase structure of egg phosphatidylcholine–cholesterol vesicles should be more difficult to determine than that of DPPC–cholesterol. This is in part because the egg phosphatidylcholine is itself a complex mixture having no well-defined structural transitions in the temperature range of interest. Nonetheless, the wide use of egg phosphatidylcholine as a model system prompted us to consider its interaction with cholesterol. Fortunately, a reasonable interpretation of the results may be offered through comparison with our results for DPPC–cholesterol.

Two sets of observations provide evidence for structural changes in egg phosphatidylcholine–cholesterol vesicles. First, the variation of DPH fluorescence anisotropy with membrane cholesterol content (Figure 8) showed inflections at about 17 and 36 mol % cholesterol at 15, 25, and 37 °C. This is similar to the behavior of DPH anisotropy at 49 °C in DPPC–cholesterol vesicles (Figure 3A). Second, the partition coefficient of DPH between egg phosphatidylcholine and cholesterol-containing vesicles remained unity up to 33 mol % cholesterol, at which composition some tendency to partition into the cholesterol-containing phase appeared at 15 °C (Table I). By 50 mol % cholesterol, there was a clear tendency to partition into the cholesterol-rich phase. This is in analogy to the tendency of DPH to partition into membranes composed of mixed $L\alpha + \Gamma$ phase (Table I). With this added information, we can speculate that the 36 mol % inflection reveals a boundary between a liquid phase and coexisting liquid and amorphous, gel-like phases. Finally, the 17 mol % cholesterol inflection in Figure 8 could be due to a region of liquid-phase immiscibility, but proof of this would require considerably more evidence. It is of interest that Rubenstein et al. (1979) have reported a sudden drop in lipid lateral diffusion coefficient at about 17–20 mol % cholesterol in egg phosphatidylcholine at 15 °C, in essential agreement with our results.

Cholesterol–Phospholipid Complexes in Biological Membranes? The present study approaches this very difficult question through investigation of a widely used model system. Our results have provided a unifying interpretation for a variety of observations in the literature. This interpretation is in terms of gel state phase boundaries rather than stoichiometric complexes. Nonetheless, three of the roughly vertical phase boundaries in Figure 7C occur at compositions (20, 33, and 50 mol % cholesterol) quite close to those recently proposed to result from unique packing arrangements of cholesterol with phospholipid acyl chains (22, 31, and 47 mol %; Martin & Yeagle, 1978). These proposed cholesterol–phospholipid packing arrangements may result in the formation of thermodynamically stable complexes with these compositions. Thus, phospholipid–cholesterol complex formation could still be the underlying reason for the complicated phase structure revealed by our study.

Biological membranes, however, contain mainly liquid-crystalline rather than gel-state bilayers. To obtain information related to biological membrane structure, we must more fully understand the liquid-crystalline region of both DPPC–cholesterol and an appropriate unsaturated phosphatidylcholine–cholesterol system. The phase diagram proposed here represents an essential step in this process. Aside from offering an explanation for conflicting literature reports, it provides a guide for the study of more complex unsaturated systems. Through the study of such model membranes, we may hope to establish the principles governing the interaction of cholesterol with phospholipids in mammalian membranes.

Acknowledgments

We are indebted to Dennis Alford for technical assistance and to Drs. Allen Blaurock and Gerhard Meissner for reading

and criticizing the manuscript.

References

Albon, N., & Sturtevant, J. M. (1978) *Proc. Natl. Acad. Sci. U.S.A. 75*, 2258–2260.

Andrich, M. P., & Vanderkooi, J. M. (1976) *Biochemistry 15*, 1257–1261.

Barenholz, Y., Gibbes, D., Litman, B. J., Goll, J., Thompson, T. E., & Carlson, F. D. (1977) *Biochemistry 16*, 2806–2810.

Chadha, J. S. (1970) *Chem. Phys. Lipids 4*, 104–108.

Chen, P. S., Jr., Toribara, T. Y., & Warner, H. (1956) *Anal. Chem. 28*, 1756–1758.

Costello, M. J., & Gulik-Krzywicki, T. (1976) *Biochim. Biophys. Acta 455*, 412–432.

Demel, R. A., & DeKruijff, B. (1976) *Biochim. Biophys. Acta 457*, 109–132.

Engelman, D. M., & Rothman, J. E. (1972) *J. Biol. Chem. 247*, 3694–3697.

Estep, T. N., Mountcastle, D. B., Biltonen, R. L., & Thompson, T. E. (1978) *Biochemistry 17*, 1984–1989.

Fahey, P. F., & Webb, W. W. (1978) *Biochemistry 17*, 3046–3053.

Gebhardt, C., Gruler, H., & Sackmann, E. (1977) *Z. Naturforsch. C 32*, 581–596.

Gordon, P. (1968) *Principles of Phase Diagrams in Materials Systems*, McGraw-Hill, New York.

Gulik-Krzywicki, T., & Costello, M. J. (1978) *J. Microsc. (Oxford) 112*, 103–113.

Haberkorn, R. A., Griffin, R. G., Meadow, M. D., & Oldfield, E. (1977) *J. Am. Chem. Soc. 99*, 7353–7355.

Huang, C., Sipe, J. P., Chow, S. T., & Martin, R. B. (1974) *Proc. Natl. Acad. Sci. U.S.A. 71*, 359–362.

Jacobs, R., & Oldfield, E. (1979) *Biochemistry 18*, 3280–3285.

Janiak, M. J., Small, D. M., & Shipley, G. G. (1976) *Biochemistry 15*, 4575–4580.

Kawato, S., Kinosita, K., Jr., & Ikegami, A. (1977) *Biochemistry 16*, 2319–2324.

Kawato, S., Kinosita, K., Jr., & Ikegami, A. (1978) *Biochemistry 17*, 5026–5031.

Klein, R. A. (1970) *Biochim. Biophys. Acta 210*, 486–489.

Ladbrooke, B. D., Williams, R. M., & Chapman, D. (1968) *Biochim. Biophys. Acta 150*, 333–340.

Lee, A. G. (1976) *FEBS Lett. 62*, 359–363.

Lentz, B. R., Barenholz, Y., & Thompson, T. E. (1976) *Biochemistry 15*, 4521–4528, 4529–4536.

Lentz, B. R., Freire, E., & Biltonen, R. L. (1978) *Biochemistry 17*, 4475–4480.

Lentz, B. R., Moore, B. M., & Barrow, D. A. (1979) *Biophys. J. 25*, 489–494.

Lippert, J. L., & Peticolas, W. L. (1971) *Proc. Natl. Acad. Sci. U.S.A. 68*, 1572–1576.

Luna, E. J., & McConnell, H. M. (1977) *Biochim. Biophys. Acta 446*, 381–392.

Mabrey, S., & Sturtevant, J. M. (1976) *Proc. Natl. Acad. Sci. U.S.A. 73*, 3862–3866.

Mabrey, S., Mateo, P. L., & Sturtevant, J. M. (1978) *Biochemistry 17*, 2464–2468.

Martin, R. B., & Yeagle, P. L. (1978) *Lipids 13*, 594–597.

Mueller, M., Meister, N., & Moor, H. (1980) *J. Microsc. (Oxford)* (in press).

Newman, G. C., & Huang, C. (1975) *Biochemistry 14*, 3363–3370.

Opella, S. J., Yesinowski, J. P., & Waugh, J. S. (1976) *Proc. Natl. Acad. Sci. U.S.A. 73*, 3812–3815.

Phillips, M. C., & Finer, E. G. (1974) *Biochim. Biophys. Acta 356*, 199–206.

Robles, E. C., & Van den Berg, D. (1969) *Biochim. Biophys. Acta 187*, 520–526.

Rubenstein, J. L. R., Smith, B. A., & McConnell, H. M. (1979) *Proc. Natl. Acad. Sci. U.S.A. 76*, 15–18.

Schreier-Muccillo, S., Marsh, D., Dugas, H., Schneider, H., & Smith, I. C. P. (1973) *Chem. Phys. Lipids 10*, 11–27.

Schwenk, E., & Werthessen, N. T. (1952) *Arch. Biochem. Biophys. 40*, 334–341.

Shimshick, E. J., & McConnell, H. M. (1973) *Biochem. Biophys. Res. Commun. 53*, 446–451.

Shinitzky, M., Dianoux, A.-C., Gitler, C., & Weber, G. (1971) *Biochemistry 10*, 2106–2113.

Singleton, W. S., Gray, M. S., Brown, M. L., & White, J. L. (1965) *J. Am. Oil Chem. Soc. 42*, 53–56.

Sklar, L. A., Miljanich, G. P., & Dratz, E. A. (1979) *Biochemistry 18*, 1707–1716.

Stockton, G. W., & Smith, I. C. P. (1976) *Chem. Phys. Lipids 17*, 251–263.

Stoffel, W., Chu, F., & Ahrens, E. H., Jr. (1959) *Anal. Chem. 31*, 307–308.

Tardieu, A., Luzzati, V., & Reman, F. C. (1973) *J. Mol. Biol. 75*, 711–733.

Verkleij, A. J., Ververgaert, P. H. J. Th., deKruyff, B., & Van Deenen, L. L. M. (1974) *Biochim. Biophys. Acta 373*, 495–501.

Ververgaert, P. H. J. Th., Verkleij, A. J., Elbers, P. F., & Van Deenen, L. L. M. (1973a) *Biochim. Biophys. Acta 311*, 320–329.

Ververgaert, P. H. J. Th., Verkleij, A. J., Verhoeven, J. J., & Elbers, P. F. (1973b) *Biochim. Biophys. Acta 311*, 651–654.